Multiscale multifractal analysis of heart rate variability recordings with a large number of occurrences of arrhythmia

J. Gierałtowski,[1,*] J. J. Żebrowski,[1] and R. Baranowski[2]
[1]*Faculty of Physics, Warsaw University of Technology, Warsaw, Poland*
[2]*The Cardinal Stefan Wyszyński Institute of Cardiology, Warsaw, Poland*
(Received 13 June 2011; revised manuscript received 22 December 2011; published 17 February 2012)

Human heart rate variability, in the form of time series of intervals between heart beats, shows complex, fractal properties. Recently, it was demonstrated many times that the fractal properties vary from point to point along the series, leading to multifractality. In this paper, we concentrate not only on the fact that the human heart rate has multifractal properties but also that these properties depend on the time scale in which the multifractality is measured. This time scale is related to the frequency band of the signal. We find that human heart rate variability appears to be far more complex than hitherto reported in the studies using a fixed time scale. We introduce a method called multiscale multifractal analysis (MMA), which allows us to extend the description of heart rate variability to include the dependence on the magnitude of the variability and time scale (or frequency band). MMA is relatively immune to additive noise and nonstationarity, including the nonstationarity due to inclusions into the time series of events of a different dynamics (e.g., arrhythmic events in sinus rhythm). The MMA method may provide new ways of measuring the nonlinearity of a signal, and it may help to develop new methods of medical diagnostics.

DOI: 10.1103/PhysRevE.85.021915 PACS number(s): 87.19.Hh, 87.10.Ca

I. INTRODUCTION

One way of determining the nonlinear properties of phenomena such as human heart rate variability is to study its fractal properties [1–7]. In practice, we look for characteristic exponents that describe the scaling of the fluctuations of the signal [8]. In the case of a monofractal time series, the fluctuation scaling may be described by a single exponent H (the Hurst exponent) [9,10]. But there is a class of signals that are much more complex and whose fractal properties vary from point to point along the time series [11]. Such signals require not only one but a whole spectrum of local Hurst exponents h and are called multifractal. In a simple description, a time series is multifractal if its fluctuations of different magnitude have different scaling exponents, and such a wide range of scaling exponents is preserved for every reasonably long part of the time series.

In the literature, one can find many examples of multifractal scaling of fluctuations in time series of very different phenomena: human gait [12], earthquake-related geoelectrical data [13], or even in the structure of music tracks [14]. Due to its universality and the not always clear reasons for the occurrence of multifractality, this seems to be a very promising area of research with great potential. For example, multifractal analysis indicates the loss of variability of the heart rate of subjects with congestive heart failure [5], and it allows to assess the antagonistic behavior of the branches of the heart rate controlling systems [4] and to demonstrate the differences between the heart rate variability of healthy persons and that of patients with hypertrophic cardiomyopathy [7]. In spite of the successes noted in the literature, multifractal analysis is in need of further study and refinement. This is because the comparison of different implementations of such analysis indicates serious limitations stemming from basic assumptions about, e.g., nonstationarity and the acceptable level of noise in the signal.

For some time now, our group has been developing methods to assess the properties of heart rate variability for medical diagnostic purposes [15–21]. The main focus in such assessments is, usually, the properties of the sinus rhythm of the heart, i.e., heart rhythm that originates in the normal functioning of the electrical conduction system of the heart [22]. It is widely accepted that the properties of sinus rhythm are the result of the state of the systems controlling the heart rate variability—mainly the state of the autonomic nervous system, which is one of the main targets for medical diagnostics. The difficulty lies in the fact that clinical patients, who should be the target, have a sinus rhythm with many inclusions from heart beats originating outside the electrical conduction system (different forms of arrhythmia) interspersed between normal heart beats. In some cases, the variability of the sinus rhythm may be unusually low and the apparent large heart rate variability is mainly due to arrhythmia. Many linear and nonlinear signal analysis methods are vulnerable to such kinds of nonstationarities. Consequently, many studies—including those using monofractal and multifractal analysis—focus on heart rate variability that contains not more than 5% of arrhythmia, or they use algorithms to filter arrythmic heartbeats (compare the medical data description in Ref. [5]) ,rendering their use in a clinical setting doubtful.

The starting point for our studies was curiosity: how sensitive indeed is multifractal analysis to nonstationarities in the heart rate time series, such as arrhythmia? We looked for a way that could provide a reliable analysis of a signal with a large number of occurrences of arrhythmia, without the need to filter it out or any interpolation.

In Sec. II, we briefly discuss multifractal detrended fluctuation analysis. In Sec. III, we discuss the medical data used to develop our method and the artificial test series used in the paper. In Sec. IV, we describe the analysis of the standard

*gieraltowski@if.pw.edu.pl

multifractal detrended fluctuation analysis (MF-DFA) method. Section V describes the multiscale multifractal method introduced here and its advantages. Section VI contains a description of the relation of the multiscale multifractal analysis (MMA) to earlier methods, including the effects of destroying correlations within the time series, the length of the analyzed time series, noise in the data, and the effect of nonstationarity in the form of inclusions of a dynamics different from the rest of the series. This part of the paper is focused on the analysis of natural (sinus) heart rhythm with many arrhythmic events included. We show that the new method is able to characterize monofractality or multifractality of time series in a wide range of frequencies (scales) simultaneously and is hence quite resistant to such nonstationarities.

II. MULTIFRACTAL DETRENDED FLUCTUATION ANALYSIS

Multifractal detrended fluctuation analysis, which was developed by Kantelhardt *et al*. [23], is an effective numerical method to examine the scaling properties of fluctuations by calculating a set of multifractal fluctuation functions $F_q(s)$. First, we have to divide the time series of length N into series of contiguous windows of length s [the number of contiguous windows is $N_s \equiv \mathrm{int}(N/s)$]. Since s in usually not a divisor of the length of the time series, there are parts at the end of the time series that would be omitted. To avoid such a situation, we prepare again a series of contiguous windows of length s, but this time starting from the end of the time series (together we obtain $2N_s$ windows). The fluctuations are measured as sums of squares of local differences between the time series integrated over the time and a detrending polynomial fit to the data within the given window. For $\nu \in \langle 1, N_s \rangle$, we have

$$F^2(\nu,s) \equiv \frac{1}{s}\sum_{i=1}^{s}\{Y[(\nu-1)s+i] - y_\nu(i)\}^2 \qquad (1)$$

and for $\nu \in \langle N_s+1, 2N_s \rangle$,

$$F^2(\nu,s) \equiv \frac{1}{s}\sum_{i=1}^{s}\{Y[N-(\nu-N_s)s+i] - y_\nu(i)\}^2, \qquad (2)$$

where s denotes scale (window width), $Y(j)$ is the data profile (the integrated series), ν is the current window number, and y_ν is the polynomial fit within the current window ν. The fluctuations $F^2(\nu,s)$ are used to determine the fluctuation functions $F_q(s)$,

$$F_q(s) \equiv \left\{\frac{1}{2N_s}\sum_{\nu=1}^{2N_s}[F^2(\nu,s)]^{\frac{q}{2}}\right\}^{\frac{1}{q}}, \qquad (3)$$

where q is a parameter. The order of fluctuation parameter q allows us to focus the analysis on different magnitudes of the observed fluctuations, i.e., for $q < 0$, mainly small fluctuations are analyzed, while for $q > 0$, mainly large fluctuations are analyzed. The power-law scaling function in the form

$$F_q(s) \sim s^{h(q)} \qquad (4)$$

lets us easily determine the generalized Hurst exponent $h(q)$ as a function of the magnitude of the fluctuations. Values of h are interpreted as follows [12,24]: $h \in (0,0.5)$ indicates antipersistency of the time series, $h = 0.5$ indicates uncorrelated noise, $h \in (0.5,1)$ indicates persistency of the time series, $h = 1.5$ indicates Brownian motion (integrated white noise), and $h \geqslant 2$ indicates black noise. In the next step, applying the Legendre transform to $h(q)$, the singularity spectrum $f(\alpha)$ is usually obtained. The singularity spectrum is a very compact and popular way of presenting the fractal properties of a time series [5–7,13,14,25]. But because of the problems described below, we are not going to use the singularity spectrum $f(\alpha)$. It is important to remember that, as noted in Ref. [23], one does not study here the fractality (or, to be more precise, the self-similarity) of a two-dimensional plot of a time series (at least because the vertical and horizontal axis contents are not comparable) but rather a one-dimensional structure of points each with a value assigned.

There seem to be two main sources of multifractality of a time series [23,26]: the occurrence of nonlinear correlations and fat-tailed probability distributions of the data (or increments of the data) in the series. The two reasons may have a different share in generating the multifractality of a signal.

There are many factors that may artificially increase the change of the calculated h as a function of q indicating an apparent multifractality, e.g., observational noise, strong trends, and the precision of the calculations. Consequently, we consider every time series for which $\Delta h \leqslant 0.2$ to be monofractal and only the time series with $\Delta h > 0.2$ as multifractal.

III. DATA

Heart rate variability data were extracted from 24-hour Holter ECG recordings using the 563 Strata Scan Del Mar Avionics system. The Holter recordings are all part of an anonymous Holter ECG database of the Institute of Cardiology (Warsaw, Poland) and were collected for medical purposes. They are currently used for the training of doctors and medical technicians at the Institute of Cardiology. In addition to the heart rate variability recording, the data include age, sex, and the medical state of the patient only. All data were checked by a qualified cardiologist: normal beats were detected, artifacts were deleted, and arrhythmias were recognized. No arrhythmia filtering was conducted.

We analyzed 51 RR interval series, i.e., time series of intervals between consecutive heartbeats (an example of such a series is shown in Fig. 1). The RR interval time series were sampled at 128 Hz, i.e., with a resolution of 8 ms. Thus, observational errors are more than two orders of magnitude smaller than the measured signal. There were 42 time series recorded in healthy subjects and 9 obtained for subjects at risk of cardiac arrest, therein 5 had no organic heart disease, so that, in spite of previous cardiac arrest, no pathology could be recognized. The main effort in this paper is focused on the properties of the heart rate variability of healthy subjects. In addition, we were interested in checking what the multiscale multifractal properties are of cardiac arrest patients without organic heart disease (the recordings are difficult to obtain, hence the small number analyzed here). Such patients are particularly easy to miss using standard diagnostic methods in a clinical setting. The other four cardiac arrest cases (with organic heart disease) were included here because of the

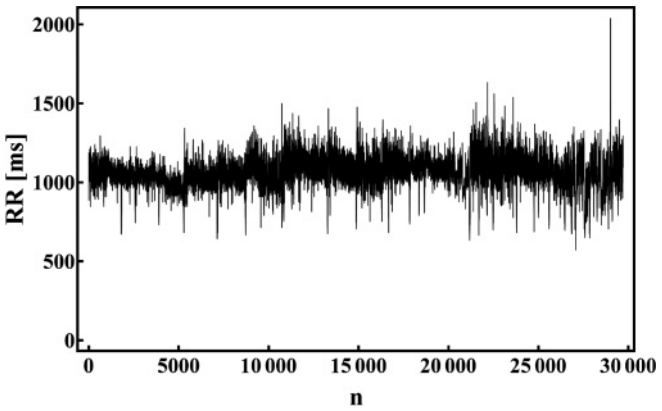

FIG. 1. Nighttime RR interval series of a healthy, 25-year-old man (subject code: CHM).

characteristic properties of their heart rate variability, which are useful for demonstration purposes. We analyzed only the nighttime parts of the recordings when the subject was asleep to avoid the effect of daytime activities on heart rate variability. Because each subject had a different time of going to sleep, in each case the period of observation was defined based on the average RR interval value (it increases markedly during sleep). Only time series longer than 9000 intervals were analyzed. In several recordings, it was necessary to remove from the time series (without replacement) abnormally long intervals (>3 s) due to artifacts or technical problems with the recognition of the R peak. The number of such removals never exceeded three in a single recording. No data filtration or averaging was applied to the RR interval series.

We generated also several artificial series: a uniformly distributed series of random numbers (range $\langle 0,2000\rangle$) and a random number Cauchy distributed series (location 0, scale 1). We generated also a deterministic and a nondeterministic binomial cascade. To do this, we divided a line segment of length 1 into two parts of equal length. We multiplied both parts by the weights m_1 and m_2 (where $m_1 + m_2 = 1$). We repeated the procedure for every line segment created in the previous step. In the case of the nondeterministic cascade, the segments were multiplied by weights in random order. In this paper, we used also a deterministic cascade formed in 14 steps, thus of length 2^{14}, with weights $m_1 = 0.25$ and $m_2 = 0.75$. We used also a modified nondeterministic cascade. Because the initial cascade distribution is asymmetric, we added to it its reversed (multiplied by -1) version, obtaining a symmetric distribution. We created also a few more artificial time series by merging the series mentioned above as described later in the text.

IV. PROPERTIES OF MF-DFA

The final results of MF-DFA depend strongly on several decisions of the user. The first problem to be considered is the subtraction of the mean $\langle x\rangle$ while calculating the data profile. Because of the detrending procedure, this step is unnecessary [23].

The second decision to be made is the choice of the order of the detrending polynomial applied within each data window to obtain $F_q(s)$. We found only slight differences in the results while using the order 1 (DFA1) and the order 2 (DFA2) polynomials to analyze the RR interval time series. Below we show results only for the order 2.

The third decision seems to be the appropriate choice of the range of scales s, for which the family of curves $F_q(s)$ should be calculated. A too large s results in the division of the time series into a too small number of windows. We found that a division into fewer than 50 data windows often causes the $F_q(s)$ curves to converge at the scale of saturation. In turn, too small scales s cause the detrending procedure to be executed on a set of only a few points. For very small scales $s < 10$, after the detrending procedure, the calculated variance often is of the order of the accuracy of the C++ data type double, which may result in an arithmetic underflow. In our tests using the RR interval series, the calculations were impossible for almost all cases for $s < 10$ because the maximal software precision was exceeded. Therefore, the often obtained drastic decrease of the values of $F_q(s)$ for $s < 10$ is a result of an arithmetic underflow (if not for all, at least for the majority of the calculation windows). That is why we set the usable range of scales to be $s \in \langle 10, \frac{N}{50}\rangle$, where N denotes the length of the time series. In the case of the nighttime RR interval series analyzed by us, N was usually about 30 000. Thus, all of our calculations were made and are presented for scales $s \in \langle 10,600\rangle$.

The slopes of the log-log fits to the family of $F_q(s)$ curves determine the local Hurst exponents and hence the $h(q)$ dependence. The details of the fitting procedure are crucial to the final results. Even small differences in realizations of this step may cause drastic changes in the outcome. The plots of $F_q(s)$ often show substantial fluctuations. As a result, the choice of even a slightly wider fitting window can give a completely different local Hurst exponent, changing the $h(q)$ curve importantly (animation 1 in Ref. [27]). We found that the effect occurs even when small changes in the fitting window size or positioning on the scale axis are made, in spite of the fact that the coefficient of determination R^2 remains large—approximately 0,98–0,99. We found this to be one of the most important effects that we considered while suggesting our new solutions.

Multifractal analysis of time series is conducted in a few steps, every one of which yields ever more highly processed results, requiring additional computations involving some subjective decisions. First of all, the plot of the fluctuation functions $F_q(s)$ is constructed. Next, derived from the $F_q(s)$ dependence, the dependence $h(q)$ of the generalized Hurst exponents on the order of fluctuation q is found. And finally, the singularity spectrum $f(\alpha)$ is calculated from the Legendre transform.

The only result in the MF-DFA method, which is only very slightly dependent on the individual decisions of the user, is the initial step, namely the computation of the family of the $F_q(s)$ curves. Because of the rather subjective decisions of the user about the details of the fitting procedures and their effect on the resultant $h(q)$ dependence, one should be careful about the way the quantitative analysis of the $h(q)$ dependence is carried out. However, the general shape of the $h(q)$ dependence is

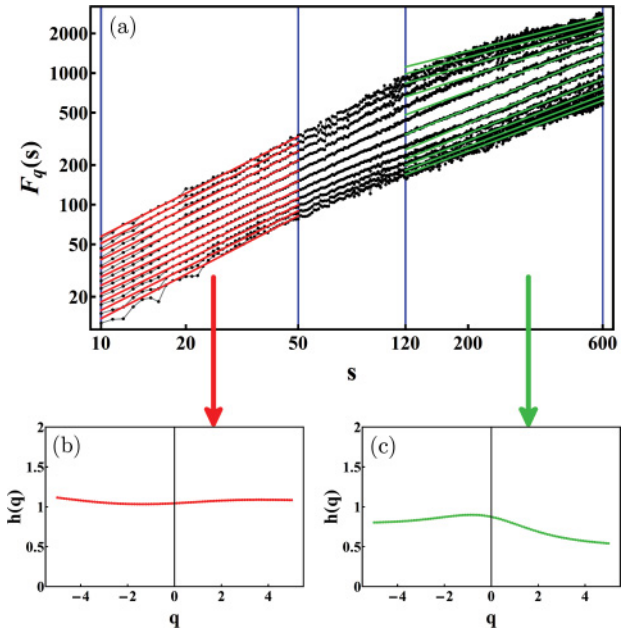

FIG. 2. (Color online) (a) Plot of the fluctuation functions $F_q(s)$ (black points) calculated for the series presented in Fig. 1. The curves correspond to q between -5 and 5 in steps of 1. Vertical (blue) lines mark two examples of the fitting windows for the small $s \in \langle 10,50\rangle$ range and for the large $s \in \langle 120,600\rangle$ range. Fits made within these two windows are shown by solid lines (red or dark gray in the left window and green or light gray in the right window). (b), (c) Two examples of the $h(q)$ curves, obtained in the fitting windows of (a), for the small and the large scales s, respectively.

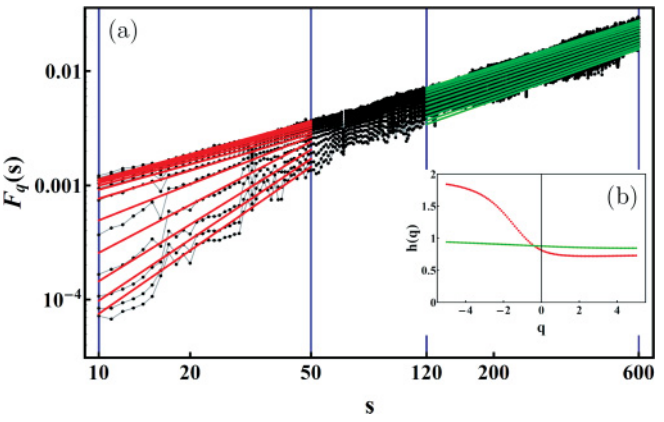

FIG. 3. (Color online) (a) Family of curves $F_q(s)$ calculated for the first test signal (multifractality visible for the small scales and monofractality for the larger scales). Vertical (blue) lines mark two examples of the fitting windows for the small $s \in \langle 10,50\rangle$ range and for the large $s \in \langle 120,600\rangle$ range. Fits made within these two windows are shown by solid lines (red or dark gray in the left window and green or light gray in the right window). (b) The $h(q)$ dependence calculated for the small (red or dark gray points, upper curve) and for the large (green or light gray points, lower curve) scales s.

qualitatively stable and remains the clearest way of detecting the monofractality or multifractality of the time series.

The singularity spectrum $f(\alpha)$, on the other hand, is calculated from the $h(q)$ dependence (vulnerable to all the procedure details described above) with the use of the Legendre transform, which amplifies some types of errors [mainly because of the presence in it of the derivative $h'(q)$]. Consequently, the singularity spectrum $f(\alpha)$ may be an unstable result, often affected by very serious artifacts that may cause difficulties and ambiguities in interpretation [7]. There seems to be no effective way of removing such artifacts. This led us to the conclusion that a reliable singularity spectrum $f(\alpha)$ is very difficult to obtain and that it should be treated only as an additional, indicatory result.

A problem that seems even more serious but also far more interesting is the presence of the crossover, i.e., the change of the average slope of the $F_q(s)$ at some scale s, in the results obtained from the RR interval series (Fig. 2).

A constant $h(q)$ indicates monofractality, while multifractality is associated with a wide range of values of $h(q)$ [23]. In the case of RR interval series studied here (Fig. 2, other examples shown below), the results of the procedure are complex, i.e., there is a different shape of the $h(q)$ curve for small and large scales s, indicating different fractal properties for small and large scales s. It is thus possible to observe, e.g., monofractal properties in small scales and multifractal properties in large scales for the same time series.

The crossover effect is sometimes interpreted as the result of the use in the analysis of a too narrow window of data (finite scale size effect) [28,29]. But it is also interpreted as a result of different correlation properties for small and large scales in the signal [30–32] (in the case of heart rate variability data, the latter phenomenon may be interpreted as an effect of respiration on the heart rate [33]). We agree with both interpretations: for the lowest possible scales $s < 10$, arithmetic underflow often occurs; for scales from the range $s \in \langle 10,50\rangle$, the scaling properties are due to short-range correlations; and for scales $s > 50$, the scaling properties are due to long-range correlations (ranges approximate). These two concepts, together with the notion that multifractality is caused by long-range correlations, could be the reason for the rejection of the results obtained for low scales s by some authors [7,29]. The position of the crossover may depend on q [31,32], which also causes additional interpretation problems.

We attempted to find out whether indeed the calculation of the multifractal properties at the lower end of scales ($s \in \langle 10,50\rangle$) does not yield usable results. To illustrate where our doubts in this matter come from, we prepared two test series (Figs. 3 and 4). To generate the time series for both examples, we need to merge together two time series: a monofractal series of random numbers and the multifractal binomial cascade (Sec. III). In the first example (Fig. 3), we generated the binomial cascade. Then we removed from the series all values $<0.000\,01$ (because the values in the binomial cascade series form characteristic discrete levels, this means we left only a few of the largest elements of the series). In their place, we substituted uniformly distributed random numbers from the range $\langle 0,0.006\rangle$ (similar to the largest values in the binomial cascade). As a result, we obtained a binomial cascade embedded in noise. Analysis of such a signal shows its multifractal nature for small scales, but for larger scales the effect of noise becomes clearly visible and monofractality prevails. In the second example (Fig. 4), we used once more the binomial cascade replacing every point x_i by 100 points generated using the formula $x_i r$, where r denotes a random

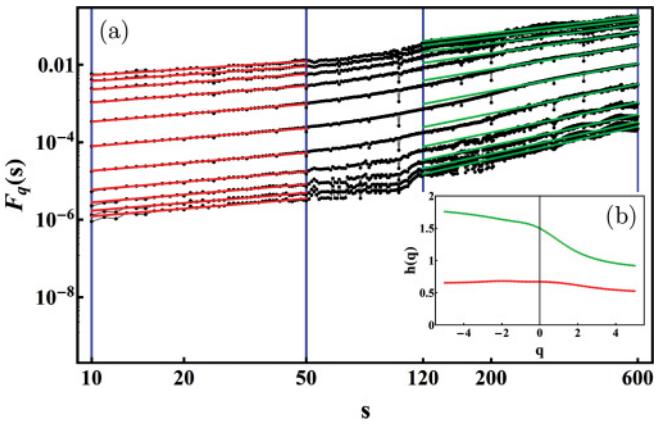

FIG. 4. (Color online) (a) Family of curves $F_q(s)$ calculated for the second test signal (monofractality visible in the small scales and multifractality in the large scales). (b) The $h(q)$ dependence calculated for the small (red or dark gray points, lower curve) and for the large (green or light gray points, upper curve) scales s.

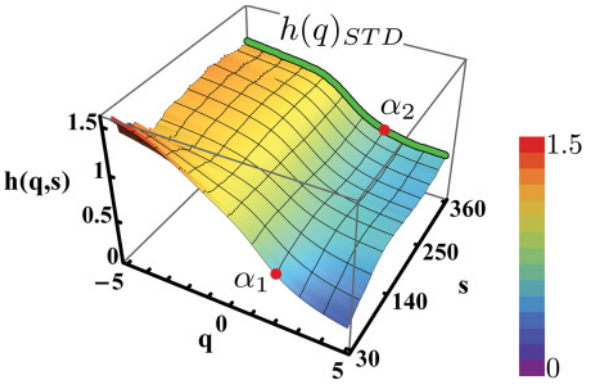

FIG. 5. (Color online) $h(q,s)$ dependence (Hurst surface) calculated for a multifractal nondeterministic binomial cascade of length 32 768. The two red (dark gray) points correspond to α_1 and α_2 calculated using the standard, monofractal DFA method. The green (light gray) line at the back of the plot corresponds to $h(q)$ calculated with the standard MF-DFA method.

number (uniform distribution) from the range $\langle 0,2\rangle$. Such a series has inverted properties with respect to the previous one, i.e., monofractality in the small scales and multifractality in the large scales.

We summarize the results obtained for the test signals as follows:

(i) We generated time series that have monofractal or multifractal properties depending on the scale of analysis s. We were able to easily detect this effect.

(ii) We reconstructed the crossover phenomena and confirmed that essential changes of fractal properties are possible within one time series, depending on the scale of analysis s (compare also [30–32]).

(iii) We were able to recognize monofractality or multifractality for small scales $s \in \langle 10,50\rangle$ (contrary to the conclusions about the ranges of interest in Refs. [7,29]).

Although the method does have lower accuracy for scales $s < 50$ [28], it is still able to easily distinguish monofractal from multifractal properties of the signal judging by the shape of $h(q)$ (Figs. 3 and 4). We see no reason to reject results obtained for scales $s \in \langle 10,50\rangle$. Consequently, we decided to analyze the multifractal properties of time series in the possibly widest range of scales, including $s \in \langle 10,50\rangle$. Moreover, crossovers often occur for small scales s and are very interesting for our research, so that the proper analysis requires an effective way of studying all available scales simultaneously and assessing the properties of the signal within the crossover region.

V. MULTISCALE MULTIFRACTAL ANALYSIS

A. Description

Castiglioni *et al.* [34] studied the effect of high altitude hypoxia on heart rate variability. The authors applied the well-known monofractal DFA method but, instead of defining fixed scale ranges, they varied continuously the scale for which they calculated the DFA exponent $\alpha_{\mathrm{DFA}}(s)$. Inspired by their work and encouraged by the results, we decided to go further and calculate a multifractal spectrum with a variable scale range.

We used a moving fitting window, sweeping through all the range of the scales s along the $F_q(s)$ plot. This allows us to study quasicontinuous changes of the $h(q)$ dependence versus the range of the scale s and as a result to obtain the generalized dependence $h(q,s)$ (a Hurst surface, Fig. 5). Because the fluctuation functions $F_q(s)$ are presented in log-log coordinates, the moving fitting window expands logarithmically, so that it seems to be of constant width (Animation 2 in Ref. [27]).

The fit is made only for points currently inside the moving fitting window. The starting width of the window includes the scales $s \in \langle 10,50\rangle$ [cf. Figs. 2(a) and 2(b)], and then the window is moved and expanded to reach the final width $s \in \langle 120,600\rangle$ [cf. Figs. 2(a) and 2(c)]. If possible, at least the first and the last fitting window should not contain the crossover, otherwise the Hurst surface will not show all possible scalings (of course, in the case of extremely short time series or wide crossovers, that is impossible). The scale axis of the $h(q,s)$ plot is calibrated so as to show the center of the fitting window—it starts from $s = 30$ (i.e., the center of the initial scale range $\langle 10,50\rangle$) and ends at $s = 360$ (the center of the range $\langle 120,600\rangle$). For clarity, the points of the $h(q,s)$ graph are connected to form a colored surface. The fluctuation functions $F_q(s)$ are plotted using a logarithmic axis for the scale s, but the Hurst surface is presented using a linear axis. This should be kept in mind while interpreting the results.

As for the standard $h(q)$ dependence obtained for fixed scale ranges, the $h(q,s)$ plot for $q < 0$ corresponds to those fragments of the signal that have a low variance (small fluctuations), while for $q > 0$ the plot characterizes the signal fragments with a large variance (large fluctuations). Also, as for the standard $h(q)$, the results for $q > 0$ are much more stable and encumbered by smaller errors. That is why the results for $q < 0$ should always be used with caution.

During the calculation of $h(q,s)$, the center of the window (the average scale) and the window itself (the scale range) are changed, so for many signals the scale range s (the window size) may be related to the frequency band of the signal. As the calculation progresses, lower and lower frequency components of the signal are analyzed. Thus, the dependence

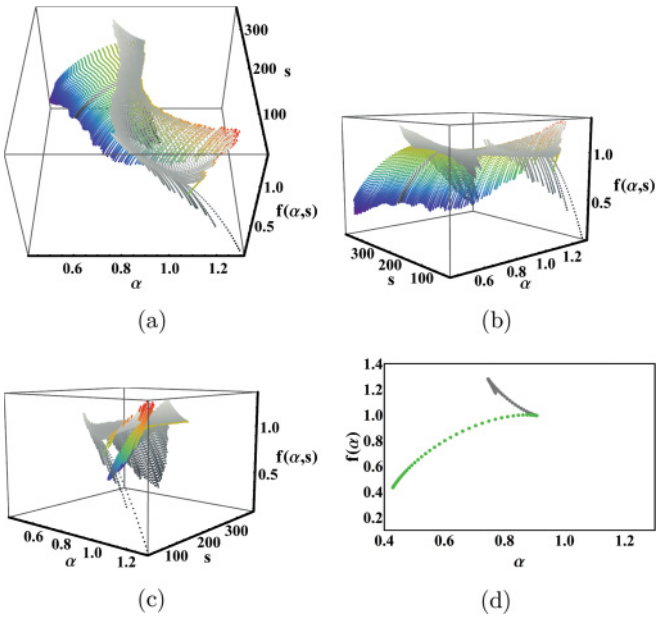

FIG. 6. (Color online) (a)–(c) The $f(\alpha,s)$ dependence for the RR interval series of the healthy subject CHM seen from three different viewing angles. Numerous artifacts make the plot difficult to read and interpret. Light gray points mark the artifacts recognized by the artifact removing procedure. (d) An example cross section of $f(\alpha,s)$ in (a)–(c) obtained for $s = 360$.

$h(q,s)$ yields information about the level of fluctuations at different frequency bands.

Just as for all other calculations of a Hurst exponent, the results can be categorized into groups [12,24]: $h \in (0,0.5)$ denotes antipersistency of the time series, $h = 0.5$ denotes uncorrelated noise, $h \in (0.5,1)$ denotes persistency of the time series, $h = 1.5$ denotes Brownian motion (integrated white noise), and $h \geqslant 2$ denotes black noise. In other words, $h(q,s)$ values correspond to types of correlations within the time series.

The natural next step after creating the generalized $h(q,s)$ dependence was to prepare also a corresponding $f(\alpha,s)$ dependence (Fig. 6). Every cross section of the $h(q,s)$ dependence, made for a particular scale s, was transformed using the Legendre transform into a cross section of the $f(\alpha,s)$ plot. As mentioned in the Introduction, calculating $f(\alpha)$ involves often the interpretation of problems due to additional artifacts specific to this calculation [7].

Although the construction of the relation $f(\alpha,s)$ is feasible in principle, we decided to analyze the properties of $h(q,s)$ first, considering such analysis less ambiguous.

B. Advantages of MMA

The generalized $h(q,s)$ dependence allows us to perform multifractal analysis without any initial assumptions about the time scale of the problem investigated, as we obtain results for many frequency bands simultaneously. The Hurst surface is also a far better way of analyzing time series with a crossover, as we do not have to avoid datasets with it or narrow the range of investigated scales only to large or only to small scales. The common practice of fixing *a priori* the scaling ranges in such methods as DFA and MF-DFA may lead to artifacts in some cases, i.e., if by mistake a crossover falls within the scaling range, the results will be biased. In the new approach described above, we obtain results for all scales present in the signal, including those for the small and large scales as well as the crossover properties. We thus avoid mistakes due to improperly predefined scaling ranges. Or, if the scaling range includes only large scales, then we miss all the information about the fractal properties in the small scales, while such properties may be dramatically different and very interesting (cf. Figs. 2–4). Even if we would try to use the standard MF-DFA method separately for the small and for the large scales, we would miss all the analysis of the properties within the crossover range, and these properties can also be very different from case to case.

In Secs. VI E and VI F, we will also show that MMA is quite resistant to observational noise and nonstationarities. The detrending inherent in MF-DFA to a large extent takes care of the nonstationarity due to relatively slow processes (i.e., trends). Another kind of nonstationarity is due to inclusions into the time series of a different dynamics (such as arrhythmic events). Because this particular kind of nonstationarity will usually affect the results only in a narrow region of the Hurst surface, leaving the other parts unaffected, the method allows us to study time series with such inclusions. This seems to be very good news for those who need to analyze RR interval series with a large number of arrhythmia episodes.

VI. RESULTS AND DISCUSSION

A. Correspondence with earlier multifractal analysis methods

We tested the multiscale multifractal analysis method in several ways. First of all, we tested it on a time series of monofractal random numbers, obtaining satisfying results. For a uniformly distributed random number series, $h(q) = 0.5$ [Fig. 7(a), [23]]. As expected, for every scale s, we obtained a flat Hurst surface [Fig. 7(b)], also situated at 0.5. For a multifractal time series of Cauchy distributed random numbers [Fig. 7(c)], also as expected, we obtained the standard shape of the multifractal $h(q)$ dependence for all available scales [Fig. 7(d)]. These two basic results show that the MMA method reproduces well the results obtained from earlier multifractal analysis methods.

B. Effect of randomization of the time series

It seems that multifractality can have two sources: nonlinear correlations and a fat-tailed probability distribution [31,32]. In the case of RR interval series, it was shown that the first source of multifractality applies and that the second one has no effect [11] as the distribution is approximately Gaussian. Thus, the characteristic shape of the Hurst surface calculated for RR interval series of a healthy man is due to correlations. In this sense, the Hurst surface is a generalized description of the correlation properties obtained from the MF-DFA method and, in general, different from that obtained by such methods as the autocorrelation function or mutual information.

To demonstrate the effect of removing the autocorrelations from the signal on MMA results, we calculated $h(q,s)$ for the nighttime RR interval series of subject CHM [Fig. 8(a)] and next for the shuffled version of this time series. In Fig. 8(b),

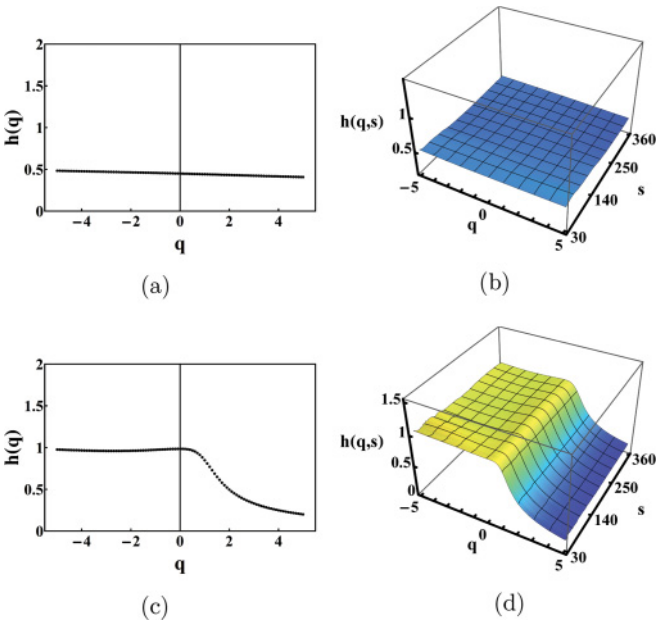

FIG. 7. (Color online) (a) The standard $h(q)$ dependence calculated using MF-DFA for a monofractal series of random numbers (uniform distribution, range $\langle 0,2000\rangle$, length of series 16 384). (b) The $h(q,s)$ dependence calculated for the monofractal series in (a). (c) $h(q)$ for a multifractal series of random numbers (Cauchy distribution, location 0, scale 1, length of series 65 536). (d) The $h(q,s)$ dependence calculated for the series in (c).

we can see that, in fact, the randomization destroyed the correlations—the results closely resemble those for white noise. Thus, we conclude that, in fact, multifractality of RR interval series is due to correlations.

C. A measure of the generalized distance between two Hurst surfaces

To reliably describe the differences between two MMA results in the next examples, we need to assess numerically a generalized, mean distance between the two $h(q,s)$ surfaces. First, we calculate the mean $\langle h(q,s)\rangle$ for each surface. Next, we adjust the values of one of the $h(q,s)$ surfaces so that the means of both surfaces are the same (by shifting the surface up or down). In this way, we were able to focus only on the differences in the shape of the surfaces independently of the change in the average Hurst exponent. We next subtracted the two surfaces from each other point by point, squared the differences, and calculated the mean. Then, we normalized the square root of the mean by dividing it by the average Hurst exponent of the first, the reference surface. This procedure may be written as follows:

$$h_{2S}(q,s) = h_2(q,s) + [\langle h_1(q,s)\rangle - \langle h_2(q,s)\rangle], \quad (5)$$

$$d = \{\langle [h_1(q,s) - h_{2S}(q,s)]^2\rangle\}^{\frac{1}{2}} [\langle h_1(q,s)\rangle]^{-1}, \quad (6)$$

where d is a measure of the mean distance between two Hurst surfaces, $h_1(q,s)$ is the reference surface, $h_2(q,s)$ is the result for the test series, and $\langle\cdots\rangle$ denotes the mean.

We set $d = 0.065$ as the threshold so that if $d \leqslant 0.065$, we consider two surfaces to be similar (i.e., indistinguishable), and if $d > 0.065$, we consider them to be different. In all

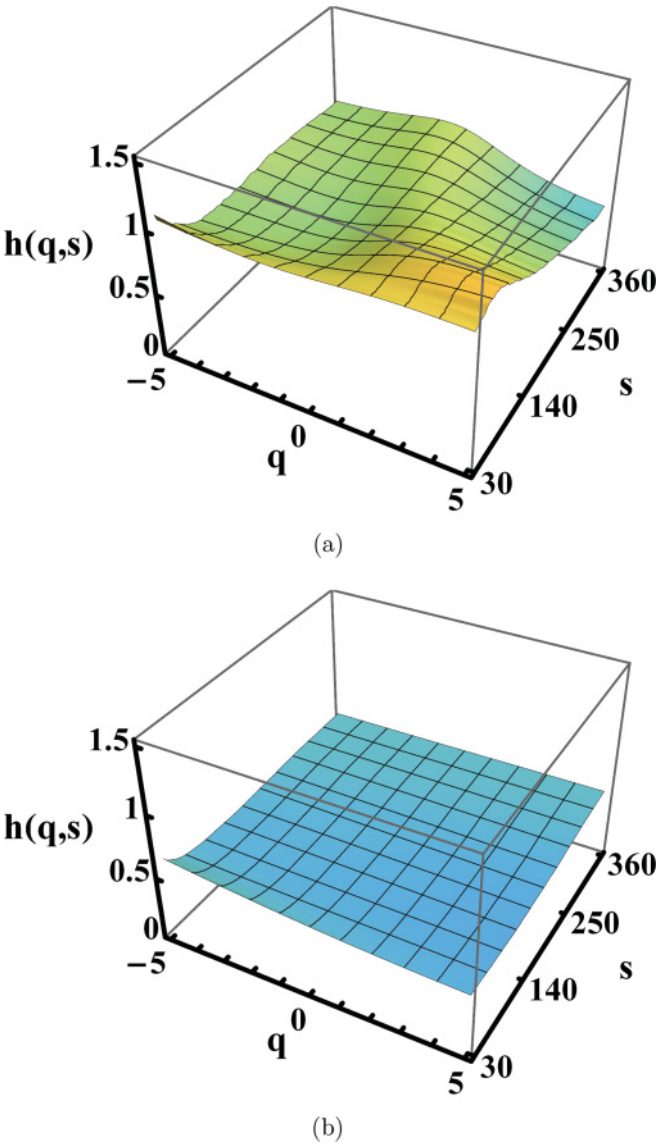

FIG. 8. (Color online) (a) The $h(q,s)$ surface calculated for the nighttime heart rate variability of a healthy 25-year-old man (CHM, length of series 29 700, cf. Fig. 1). (b) $h(q,s)$ calculated for the shuffled version of the same series.

the following examples, two reference surfaces will be used having the following mean Hurst exponents: for the healthy man, CHM $\langle h(q,s)\rangle = 0.867$, and for the Cauchy distributed random series used in all the examples, $\langle h(q,s)\rangle = 0.747$.

D. Effect of the length of the time series

Nighttime RR interval series, which are our main interest, can have very different lengths. Thus, it was important for us to find out what effect the length of the time series has on the results of MMA.

We prepared the first group of test series by selecting fragments from the RR interval series of the healthy man CHM (length of series 29 700, cf. Fig. 1) recorded during the night. Initially, we calculated $h(q,s)$ for the complete time series [Fig. 8(a)]. We prepared test time series obtained extracting 20 000, 15 000, 10 000, 7500, 5000, and 2000

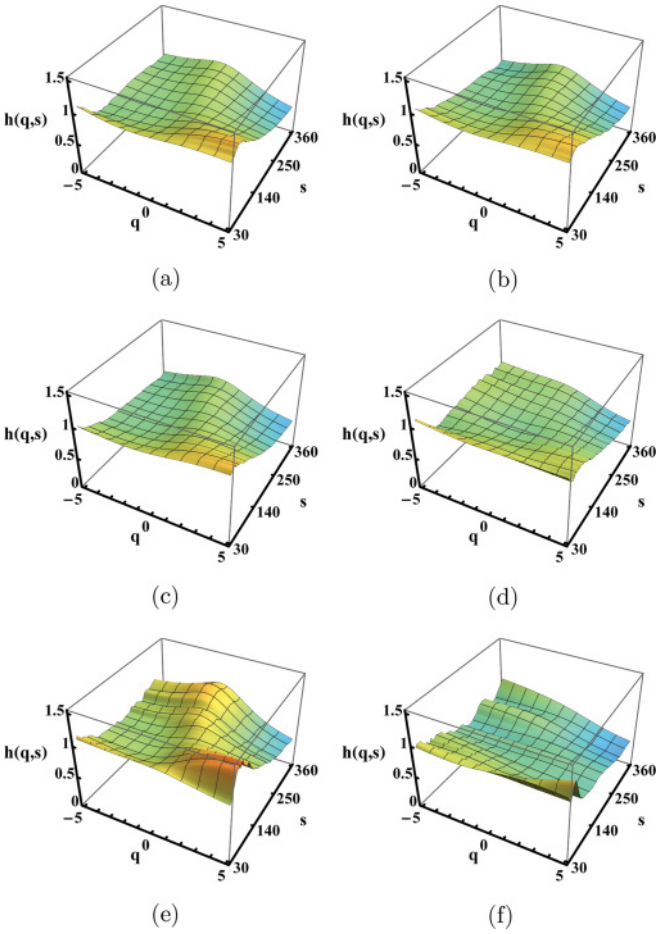

FIG. 9. (Color online) $h(q,s)$ for the RR interval series of the healthy subject CHM, shortened to different lengths: (a) 20 000, (b) 15 000, (c) 10 000, (d) 7500, (e) 5000, and (f) 2000. Presented are results averaged over 1000 realizations of the test series.

consecutive intervals from this series. The starting point for the shortened subseries was chosen randomly and all the distances d presented below are averaged over 1000 realizations of the extraction procedure and presented together with the standard deviation of the results.

The results (Fig. 9) for the series of length 20 000 are very similar to these for the whole available series [length 29 700, Fig. 8(a)]. The results for 15 000 and 10 000 are still very similar, but the results for the series length 7500 are different. For even shorter time series, the changes were even more pronounced. In Table I, we can see the generalized distances between the $h(q,s)$ surface for the full length time series and that for the short fragments (cf. Sec. VI C). The mean distances between the results (taking into account the standard deviation) for the original series and the series of lengths 20 000 and 15 000 are less than 0.065, which is thus below the threshold we have assumed. The mean distance for the 10 000-interval-long series is also below the threshold, but the standard deviation σ for this case shows that some of the test series yielded $h(q,s)$, exceeding the threshold criterion of 0.065. This is then a borderline case, and nighttime RR interval series shorter than 15 000 should not, in general, be used.

As mentioned above, multifractality can have two sources: long-range correlations and a fat-tailed probability distribution

TABLE I. Mean values $\langle h_2(q,s)\rangle$ and intersurface distances d (defined in Sec. VI C) between the results for the original time series (healthy subject CHM or Cauchy distribution) and their successive modifications (shortened series, see Sec. VI D for details). In every case, the mean value μ and the standard deviation σ of the results for the 1000 realizations of each test series are given.

			20 k	15 k	10 k	7.5 k	5 k	2 k
CHM	d	μ	0.038	0.046	0.057	0.068	0.084	0.156
		σ	0.010	0.011	0.016	0.014	0.025	0.058
	$\langle h_2(q,s)\rangle$	μ	0.832	0.821	0.829	0.840	0.841	0.869
		σ	0.014	0.031	0.057	0.069	0.079	0.123
Cauchy	d	μ	0.056	0.070	0.089	0.106	0.137	0.259
		σ	0.016	0.026	0.034	0.030	0.042	0.202
	$\langle h_2(q,s)\rangle$	μ	0.755	0.755	0.757	0.760	0.766	0.791
		σ	0.015	0.018	0.030	0.039	0.058	0.114

[31,32]. In the case of non-Gaussian distributed time series, it is difficult to tell how much of the multifractal properties is due to correlations and how much is due to the properties of the distribution of the signal. In such a case, the analysis of the exact values of the Hurst surface [e.g., assessment of persistence or antipersistence by comparison of $h(q,s)$ with 0.5] does not seem to make sense. For the RR interval series, the distribution is approximately Gaussian. However, noise, seasonal trends, and other nonstationarities may affect $h(q,s)$. Below, we thus discuss the shape and the span of the Hurst surface rather than keep track of its values.

In the case of RR interval series, nonlinear correlations are the main source of multifractality. As a result, we wanted to check what impact the shortening of the series length has on our results in the case of a time series for which multifractal properties are only due to its fat-tailed distribution.

We took 20 000, 15 000, 10 000, 7500, 5000, and 2000 intervals, respectively, of the series of the Cauchy distributed random numbers used above [full length 65 536 data points, cf. Figs. 7(c) and 7(d)]. Once more the starting point of the shortened subseries was chosen randomly, and the results shown are averaged over 1000 realizations of the subseries preparation and presented together with the standard deviation of the results. Looking at the results for the series of length 20 000 [Fig. 10(a)], they appear to be almost identical to those for the reference series [cf. Fig. 7(d)]. The results for series length 15 000 and 10 000 are visibly different and for 7500 they are very different. For the two shortest series of lengths 5000 and 2000, the correct result is clearly destroyed. In Table I, only the mean distance d for the series of length 20 000 is lower than 0.065, which is thus lower than the threshold, but when combined with the standard deviation it become higher than the threshold. Therefore, for multifractality resulting from the properties of the probability distribution, series longer than 20 000 should be used.

Note that the standard deviations for both the distance d and the mean $h_2(q,s)$ are very high in the two examples. Each of the 1000 test series in these examples may have different correlation properties (the fragments of the RR series) or an insufficient statistical representation of the Cauchy distribution. This results in the large standard deviations in Table I. This is another point showing that series analyzed by

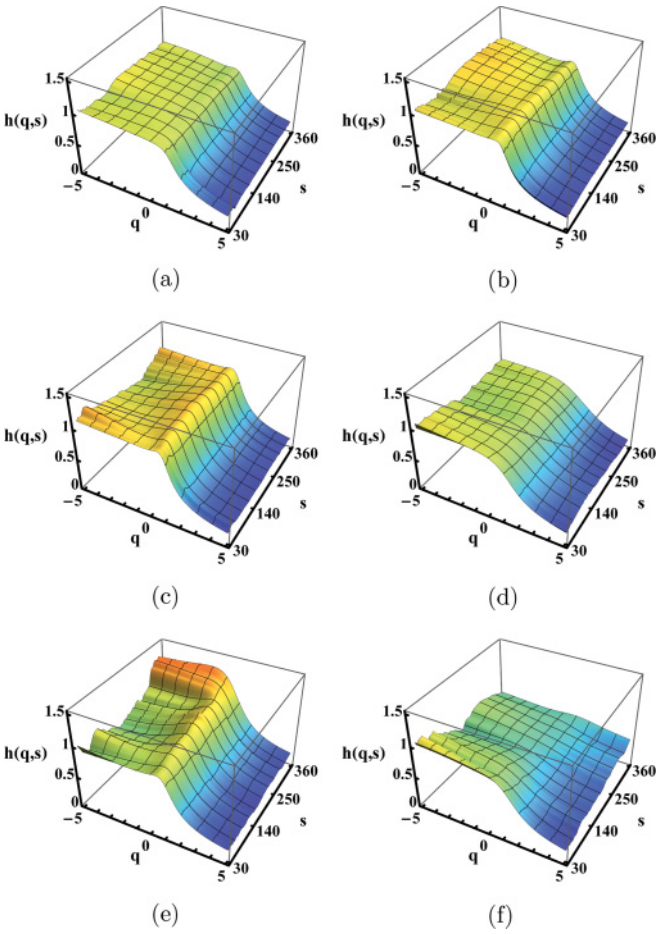

FIG. 10. (Color online) $h(q,s)$ calculated for the multifractal series of random numbers [compare with Fig. 7(d), Cauchy distribution, location 0, scale 1] of different lengths: (a) 20 000, (b) 15 000, (c) 10 000, (d) 7500, (e) 5000, (f) 2000. The presented results have been averaged over 1000 realizations of the test series.

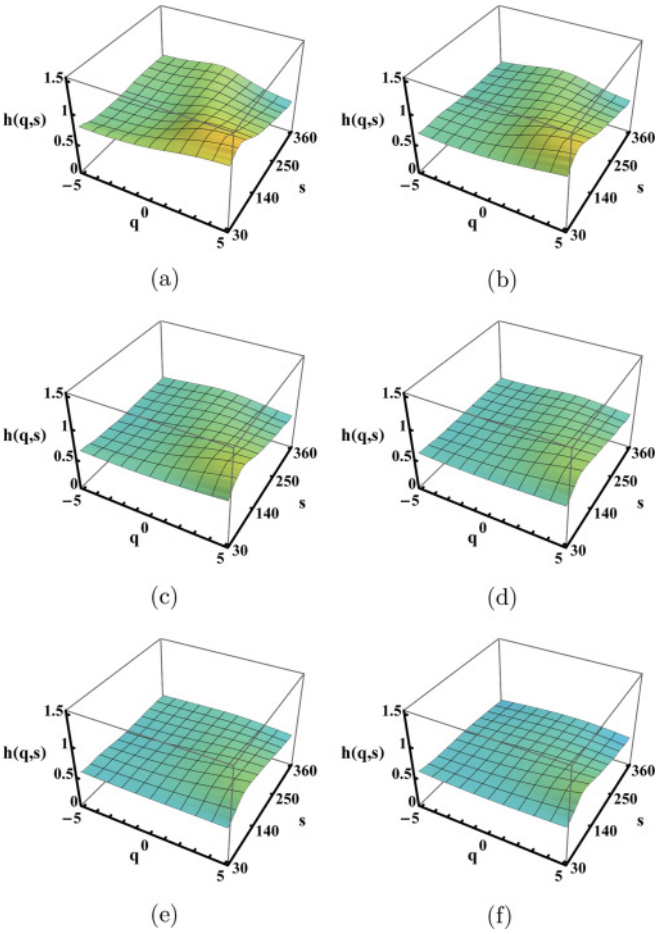

FIG. 11. (Color online) $h(q,s)$ for the RR interval series of the healthy subject CHM, with different levels of noise added: (a) 10%, (b) 20%, (c) 30%, (d) 40%, (e) 50%, and (f) 60%. The presented results have been averaged over 1000 realizations of the test series.

MMA (but also by any other multifractal method) should be sufficiently long.

For both examples (Figs. 9 and 10), for the smallest time series lengths, the Hurst surface becomes exceptionally steep and ragged. This is because the calculations of $F_q(s)$ are made using a small number of windows. Consequently, all results become much less smooth.

E. Effect of noise

Another practical matter, very important for heart rate variability analysis, is the effect of observational errors on the results of MMA. Above, we presented an example of a test series with monofractal properties at small scales and multifractal properties at large scales (Fig. 4). We suspected that it is possible to find a similar behavior, i.e., monofractality at small scales and multifractality at large scales in multifractal test signals with a high level of noise (a monofractal signal) added.

We prepared time series with different levels of noise using the equation

$$s_i = x_i(1 + np), \tag{7}$$

where s_i is the time series with noise added, x_i is the original time series, n is the level of noise (given below in percent), and p is a random number from the range $[-1,1]$. We added the simulated observation error noise at levels from 10% to 60% in steps of 10% to two test series: the RR interval series of a healthy man (CHM) and the multifractal series of Cauchy distributed random numbers. Thus, once more, we have series representing two separate sources of multifractal properties: nonlinear correlations (the RR interval series) and a fat-tailed distribution series. All results presented are averaged over 1000 realizations of series with the given level of noise and shown together with the standard deviation of the results.

For the RR interval series, 10% of noise did not change the results considerably [Fig. 11(a)]; the distance is below threshold $d = 0.059$ for this case (Table II). However, 20% of noise changes the results visibly [Fig. 11(b)]. Clearly, the general properties of the results remain the same but the range of h is smaller and therefore the measure of the intersurface distance is larger than the threshold: $d = 0.092$ (Table II). Still higher levels of noise (30%–60%) make the results resemble those for the random number series [cf. Fig. 7(b)]. Thus, for those series for which nonlinear correlations are the main source of the multifractal properties, observational errors have

TABLE II. Table showing mean values $\langle h_2(q,s)\rangle$ and intersurface distance d (defined in Sec. VI C) between the results for the original series (healthy subject CHM or Cauchy distribution) and these series with noise added, (cf. Sec. VI E for details). In every case, the mean value μ and the standard deviation σ of the results for 1000 realizations of each test series are given.

			10%	20%	30%	40%	50%	60%
CHM	d	μ	0.059	0.092	0.108	0.119	0.125	0.130
		σ	0.005	0.006	0.007	0.008	0.009	0.009
	$\langle h_2(q,s)\rangle$	μ	0.807	0.742	0.694	0.656	0.627	0.605
		σ	0.007	0.009	0.009	0.010	0.010	0.011
Cauchy	d	μ			0.030			
		σ			0.008			
	$\langle h_2(q,s)\rangle$	μ			0.754			
		σ			0.008			

a moderate impact on the results of MMA. We found also that observational noise, instead of changing the results in the smallest scales and generating a crossover effect, simply makes the results resemble those obtained for white noise at all scales.

We found the multifractality of the Cauchy distributed random numbers series to be extremely resilient to additive noise (Fig. 12, Table II): even 100% of noise added leaves the results completely intact ($d = 0.030$). In this case then, observational errors have almost no impact on the results of MMA and did not cause a crossover in the fluctuation functions $F_q(s)$ (cf. also [31]). We conclude from both examples that observational errors cannot be a source of crossover.

Adding high levels of white noise to a time series with nonlinear correlations and a normal distribution acts like randomization. As the level of noise increases, the mean $\langle h_2(q,s)\rangle$ is considerably decreased and gradually approaches 0.5, which is the result for white noise. Adding high levels of white noise to a multifractal Cauchy distributed random numbers series has no effect on the results. In both examples, the standard deviations of the intersurface distances d and the means $h_2(q,s)$ are small.

F. Effect of arrhythmia

To illustrate the effect of nonstationarity in the form of inclusions of a different dynamical behavior on MMA, we

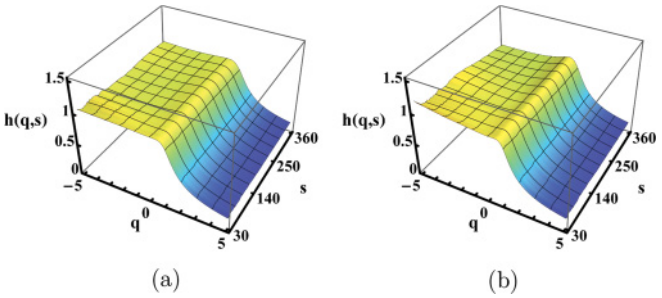

FIG. 12. (Color online) $h(q,s)$ calculated for the multifractal series of random numbers [compare with Fig. 7(d), Cauchy distribution, location 0, scale 1] with noise added: (a) 0% and (b) 100%. The results presented have been averaged over 1000 realizations of the test series.

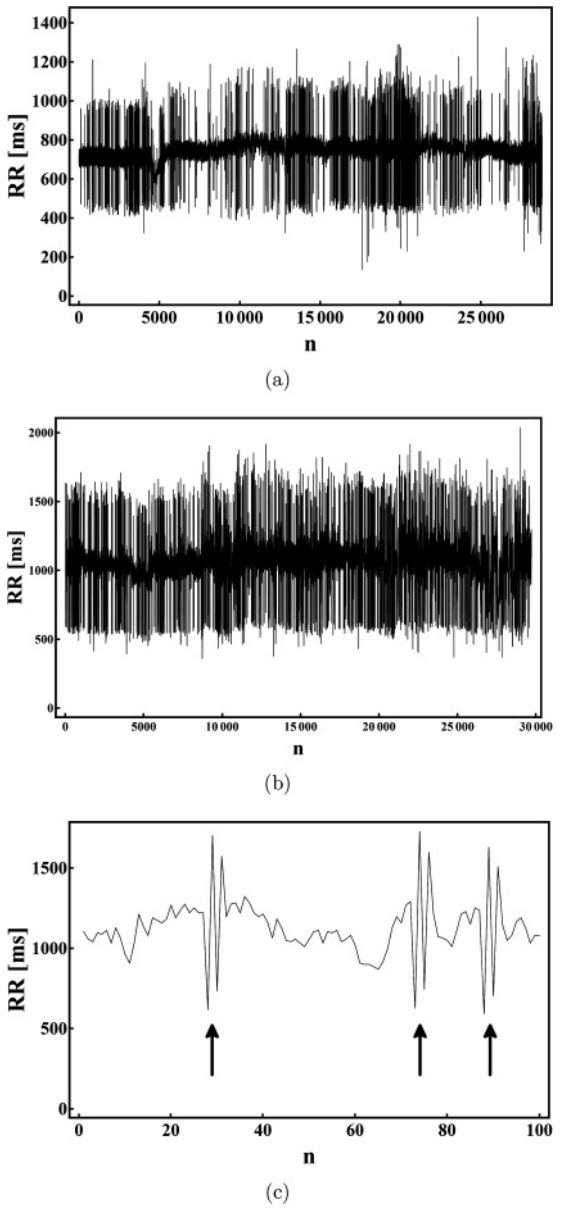

FIG. 13. (a) Nighttime RR interval series of the subject DWD, with many ectopic beats (arrhythmia). (b) The RR interval series of the subject CHM with 10% of the short arrhythmic segments incorporated. (c) Enlargement with three short, arrhythmic segments included randomly.

prepared two special examples in which we incorporated different numbers of arrhythmic events into a RR interval series measured in a healthy man.

To generate data with an adjustable number of arrhythmias, we took the RR interval time series of a 25-year-old healthy man (CHM, nighttime part 29 700 heartbeats long, cf. Fig. 1) and calculated $h(q,s)$ [cf. Fig. 8(a)]. Next, we chose the RR interval time series of a person with a relatively large number of arrhythmias [DWD, Fig. 13(a)] and extracted from it a five-heartbeats-long sample containing a typical pair of ectopic beats including the compensatory pauses. We then duplicated and incorporated the arrhythmic segment into the time series of the healthy man, putting it at random locations within the series, replacing existing intervals, obtaining 10% of

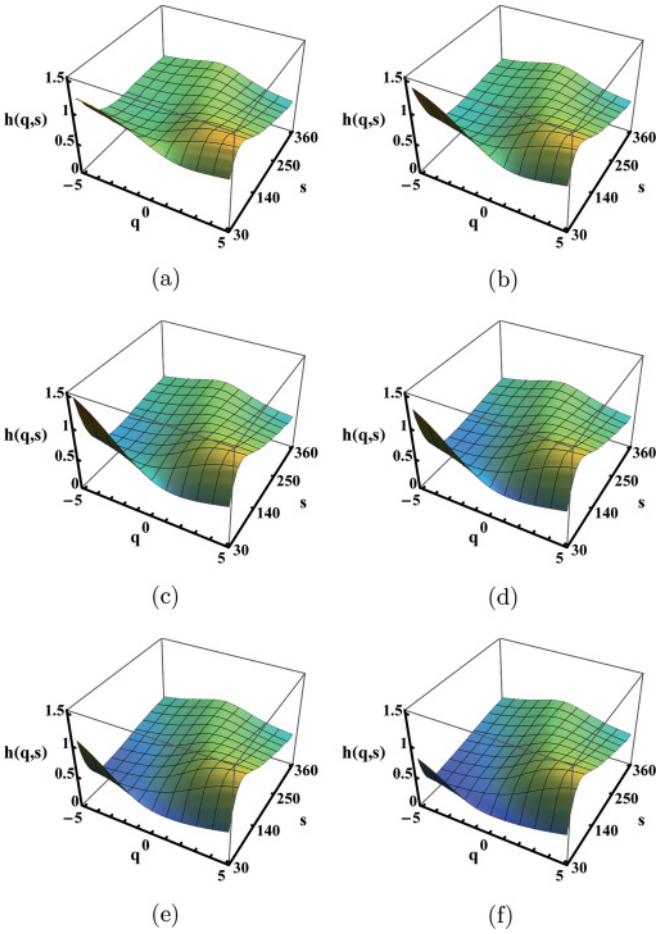

FIG. 14. (Color online) $h(q,s)$ for the RR interval series of the healthy subject CHM, with five-interval-long arrhythmic segments included: (a) 10% of arrhythmic intervals, (b) 20%, (c) 30%, (d) 40%, (e) 50%, and (f) 60%. The presented results have been averaged over 1000 realizations of the test series.

arrhythmic segments within the series [Figs. 13(b) and 13(c)]. Because the average RR interval was different in the two cases, we rescaled the implanted segments using

$$\{\widetilde{x_1},\ldots,\widetilde{x_n}\} = \{x_1,\ldots,x_n\}\frac{\langle \mathrm{RR}_H\rangle}{\langle \mathrm{RR}_D\rangle}, \tag{8}$$

where $\{\widetilde{x_1},\ldots,\widetilde{x_n}\}$ is the rescaled arrhythmic segment, $\{x_1,\ldots,x_n\}$ is the arrhythmic segment, RR_H is the RR interval of a healthy subject averaged over the length of the replaced segment, and RR_D is the RR interval of DWD averaged over the length of the incorporated arrhythmic segment. Finally, we increased the share of arrhythmic segments from 10% up to 60% (Fig. 14). For each number of incorporated arrhythmic events we generated 1000 test series, and all the results presented below are based on this data set.

We found the following:

(i) In the example using short, duplicated arrhythmic segments, 10% of arrhythmic segments incorporated into the series [Fig. 14(a)] do not change the results of MMA considerably [cf. Fig. 8(a)]; the mean distance between Hurst surfaces is equal to the threshold $d = 0.065$.

(ii) A higher incidence of arrhythmia [20% and 30%, Figs. 14(b) and 14(c)] changes the results visibly by expanding the range of $h(q,s)$ for small scales $s \in \langle 30,90\rangle$, but what is important is that at other scales, the Hurst surface is much less changed.

(iii) For 40%, 50%, and 60% [Figs. 14(d)–14(f)] of arrhythmic segments included, not only are the results for the smallest scales changed, but also all of the $h(q,s)$ dependence changes for $q < 0$.

We also prepared a second type of nonstationary data containing longer sequences of arrhythmia. Again, we extracted segments containing arrhythmia from the RR interval time series of a person with a relatively large number of arrhythmias [DWD, cf. Fig. 13(a)], but this time there were 60 independent segments, each 300 heartbeats long and thus much longer than in the first example. Such sequences containing many ectopic beats in sequences often occur in some patients [20]. The use of such longer arrhythmic segments may allow us to take into account the possibility that repeated ectopic beats have their characteristic, strong correlation properties [20]. The segments contain not only ectopic beats but also normal RR intervals. An example of such segments can be seen in Fig. 15(a). We

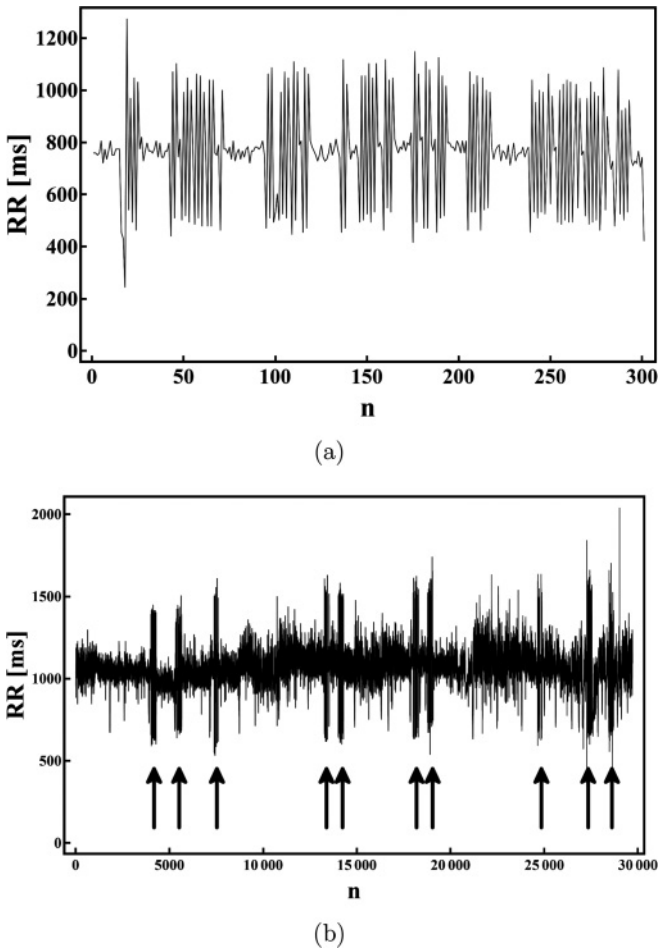

FIG. 15. (a) Example of a 300-interval-long arrhythmic segment extracted from the RR interval time series of the patient DWD, ending approximately 1 h before cardiac arrest. The arrhythmic segments were rescaled (see text) and incorporated into the RR interval series of a healthy man (CHM) at random locations. (b) RR interval series recorded for CHM with 10% of 300-interval-long arrhythmic segments incorporated (arrows).

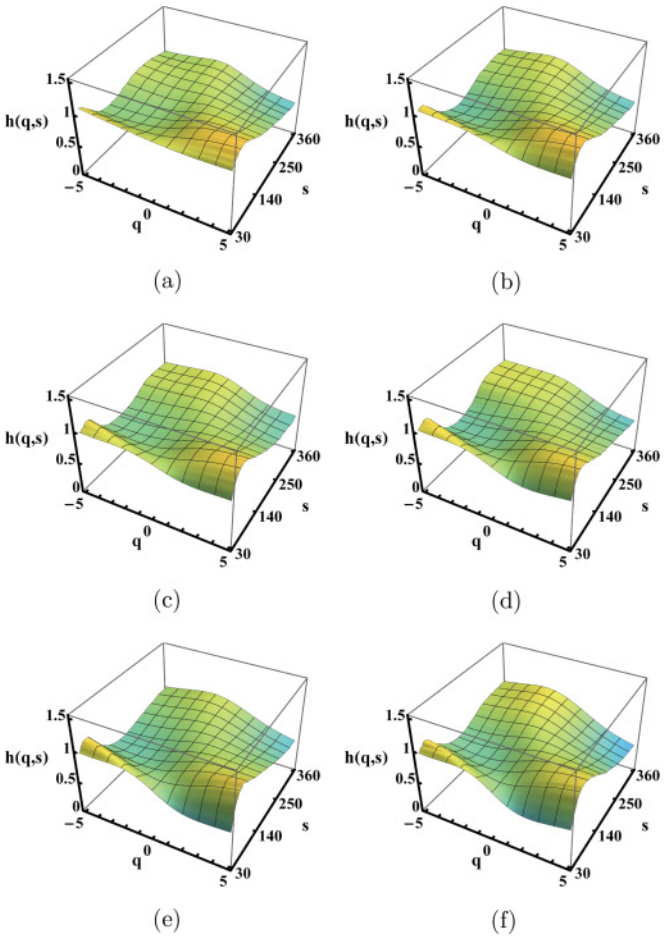

FIG. 16. (Color online) The $h(q,s)$ surface for the RR interval series of the healthy subject CHM, with 300-intervals-long arrhythmic segments added at random locations: (a) 10% of arrhythmic intervals added, (b) 20%, (c) 30%, (d) 40%, (e) 50%, and (f) 60%. The presented results have been averaged over 1000 realizations of the test series.

then incorporated 10 such arrhythmic segments into the heart rate variability time series for the healthy man CHM, obtaining approximately 10% [Fig. 15(b)] of beats within the arrhythmic segments. The segments were implanted at random times of the night into the time series. Because the average RR interval was different in the two medical cases, we rescaled the implanted segments, as described in the previous example Eq. (8). Finally, we increased the share of arrhythmic segments from 10% to 60% (Fig. 16). For each assumed number of incorporated arrhythmic segments we generated 1000 test series, and all the results presented are based on this data set. We found the following:

(i) 10% and 20% of long arrhythmic segments incorporated [Figs. 16(a) and 16(b)] does not change the results of MMA considerably [cf. Fig. 8(a)]: the mean distance between Hurst surfaces for these cases is under threshold: $d = 0.033$ and 0.061, respectively.

(ii) A large percentage of the arrhythmic segments [30% and higher, Figs. 16(c)–16(f)] causes two main changes in the shape of the Hurst surface: at small scales the surface moves downward, while it moves up for large scales and negative q.

TABLE III. Mean values $\langle h_2(q,s)\rangle$ and the intersurface distances d (see Sec. VI C for definition) between the results for the original time series (CHM) and its successive modifications (short and long arrhythmic segments included, cf. Sec. VI F). In every case, mean value μ and standard deviation σ are based on results for a group of 1000 realizations of each test series.

			10%	20%	30%	40%	50%	60%
Short	d	μ	0.065	0.109	0.142	0.169	0.194	0.216
		σ	0.004	0.003	0.003	0.002	0.002	0.002
	$\langle h_2(q,s)\rangle$	μ	0.810	0.764	0.725	0.692	0.665	0.644
		σ	0.003	0.003	0.003	0.002	0.002	0.001
Long	d	μ	0.033	0.061	0.076	0.095	0.110	0.125
		σ	0.006	0.009	0.012	0.013	0.013	0.012
	$\langle h_2(q,s)\rangle$	μ	0.856	0.847	0.852	0.842	0.834	0.825
		σ	0.009	0.013	0.015	0.016	0.018	0.018

We summarize both examples regarding the effect of arrhythmia as follows:

(i) A large part of the Hurst surface remains relatively unaffected by the inclusions of arrhythmia events in both examples, even for a very large incidence of arrhythmia: $s \in \langle 90,300\rangle$ for all values of q and $s \in \langle 300,360\rangle$ for positive values of q. If, during the calculation of the intersurface distance, the unstable parts of the Hurst surface (outside the ranges defined above) are excluded, then for the case with 30% of long arrhythmic segments incorporated into the series, the mean distance to the reference $h(q,s)$ decreases from 0.076 (cf. Table III) to 0.054, and therefore it is below the threshold.

(ii) There is a visible difference between the results obtained for the short arrhythmic inclusions and for the long ones at small scales for all values of q and for large scales and negative values of q (cf. Figs. 14 and 16). This indicates differences in correlation properties between the two examples.

(iii) Short arrhythmic segments affect much more strongly the correlation properties of the series. This is so because the long segments introduce their own correlation properties into the series [20]. The number of inclusions is also much less compared to the other test series, and so the number of transitions from the original time series to an inclusion is also smaller. The mean $\langle h_2(q,s)\rangle$ decreases significantly with the increase of the number of short segments incorporated. This effect is similar to that caused by noise or randomization.

(iv) The threshold 0.065, which we assumed for the mean distance between cases to be non-negligible, leads to the conclusions described above. Note that this is a very simple criterion and that the human eye seems to be able to discern better a part of the Hurst surface that remains invariant to nonstationarity (as well as to noise) for a larger number of arrhythmia inclusions. Perhaps a more sophisticated criterion, e.g., using an artificial neural network, would perform better. Here, we provide the simple criterion based on the intersurface distance just to show the basic properties of our method and indicate its feasibility.

G. Results for unaltered cardiological data

In this paper, we present the main properties of a new multifractal analysis method, with the ultimate goal being

to develop a universal heart rate variability analysis tool. We believe that one of the first steps on the way to clinical applications of our method should be to determine the image for healthy individuals as a reference, i.e., to determine which multifractal, multiscale properties that we can find with MMA in healthy subjects are the most characteristic for them. We carefully examined the Hurst surfaces obtained for the group of healthy subjects studied here, and we found that there are several common, typical traits (a "template"). For the healthy subjects, it appears that there is a characteristic distribution of fluctuation scaling (i.e., distribution of properties of correlations, cf. Sec. II) versus fluctuation magnitude and frequency band. The typical distribution of $h(q,s)$ values for a healthy subject (i.e., the most typical shape of the surface for such a case) can be seen in Fig. 8(a). The characteristic features are as follows:

(i) $h(q,s)$ in Fig. 8(a) varies from 0.56 to 1.16 (subject CHM, for all healthy subjects, from a minimum of 0.40–0.75 to a maximum of 1.05–1.90).

(ii) For $q > 0$ and $s \in \langle 30,90\rangle$, there is a visible hill [for CHM, $h(q,s) \approx 1.16$, and for all the group, 1.04–1.36].

(iii) Around $q = 0$ and $s \in \langle 180,360\rangle$ there is a ridge [$h(q,s) \approx 0.90$; 0.76–1.07 for all the group].

(iv) First characteristic depression for $q < 0$ and $s \in \langle 60,120\rangle$ [$h(q,s) \approx 0.81$; 0.52–0.92 for all the group].

(v) Second characteristic depression for $q > 0$ and $s \in \langle 150,360\rangle$ [$h(q,s) \approx 0.90$; 0.73–1.04 for all the group].

Any deviations from this template indicate abnormalities in the properties of heart rate variability of the recording analyzed. In particular, arrhythmic events result first of all in changes in the regions: $s \in \langle 30,90\rangle$ for all values of q and $s \in \langle 300,360\rangle$ for negative values of q.

The above-described characteristic criteria allow us to distinguish patients from healthy persons and were first applied by hand in a blind test. Note that these criteria are related to the properties and the frequency of occurrence of arrhythmia in the recordings studied (i.e., arrhythmias cause certain, abnormal changes in the Hurst surface). We also converted the above-described quantitative criteria into a numerical algorithm, which allowed us to analyze the given $h(q,s)$ automatically, and we obtained very promising statistical results. The nine cardiac arrest cases were recognized among the 49 healthy individuals with a sensitivity 78%, specificity 81%, positive predictive value 50%, and negative predictive value 94%. In particular, three of the five cardiac arrest cases without organic heart disease were properly recognized. Note that these five cases were unrecognizable by any linear method [21]. At this stage, no attempt was made to create a full-fledged assessment of the applicability for medical diagnostics with properly designed, balanced medical groups. The cardiac arrest cases were included here solely to demonstrate the properties of MMA. Thus, the sensitivity and specificity quoted here should be taken only as an indication of the potential use of our method. The method needs to be verified on a larger group of patients. In defining our "template" for healthy heart rate variability, we encountered some exceptions, usually related to the age of the subjects, especially for persons younger than 16 (see, e.g., Fig. 17) and for those older than 60.

When cross sections of the $h(q,s)$ plot for the healthy 25-year-old man CHM [Fig. 8(a)] for several constants

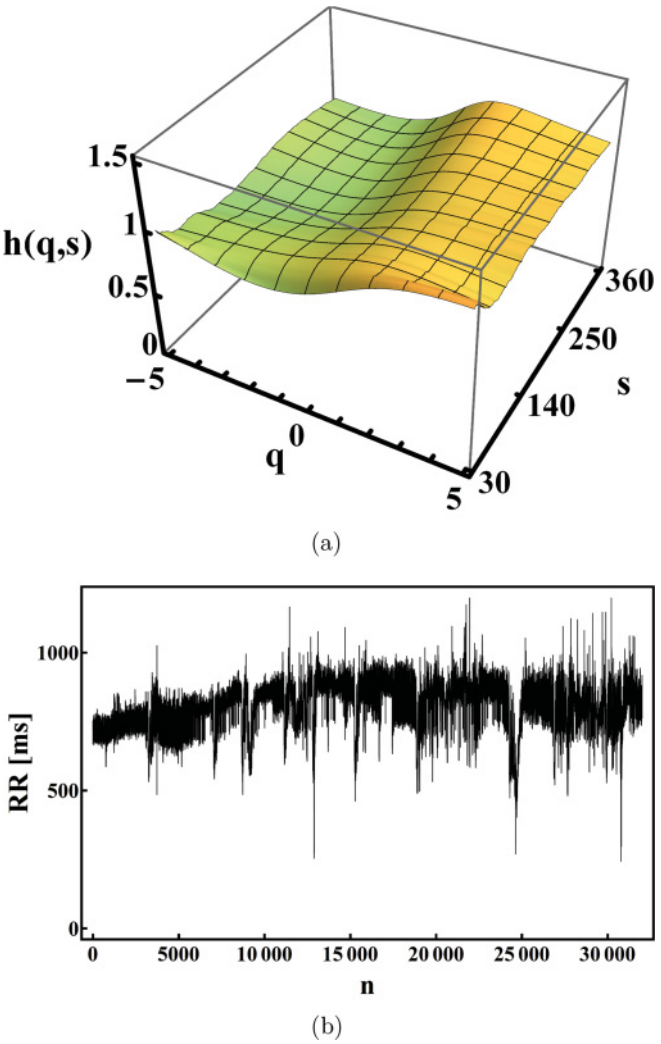

FIG. 17. (Color online) (a) "Reversed" multifractality: $h(q,s)$ calculated for the nighttime RR interval series shown below. (b) Nighttime RR interval series of a healthy 14-year-old girl (MKL).

s were analyzed, three clearly visible scaling areas ($\langle 30,50\rangle$; $\langle 50,100\rangle$; $\langle 100,360\rangle$) were found. The cross sections for the midpoints of these scaling ranges are shown in Fig. 18. This means that the fluctuation function family $F_q(s)$ for heart rate variability may exhibit a double crossover (in Fig. 18, we can see monofractality, multifractality, and "reversed" multifractality, respectively). Note that the case CHM is a typical example of heart rate variability of a healthy male in his mid-twenties.

The cross sections of $h(q,s)$ at constant s sometimes show a "reversed" multifractality, i.e., the cross section $h_s(q)$ is a monotonically increasing function [Fig. 18(b)]. This may be caused by seasonal trends in the time series or by significant changes of the fractal properties along the time series [31,32]. It is even possible to observe such "reversed" multifractality for all available scales s (nighttime RR interval series of a 14-year-old healthy girl; see Fig. 17).

Comparing Figs. 8(a) and 19(a), we can see that substantial differences are clearly visible between the results obtained for a healthy subject (CHM) and a subject without an organic

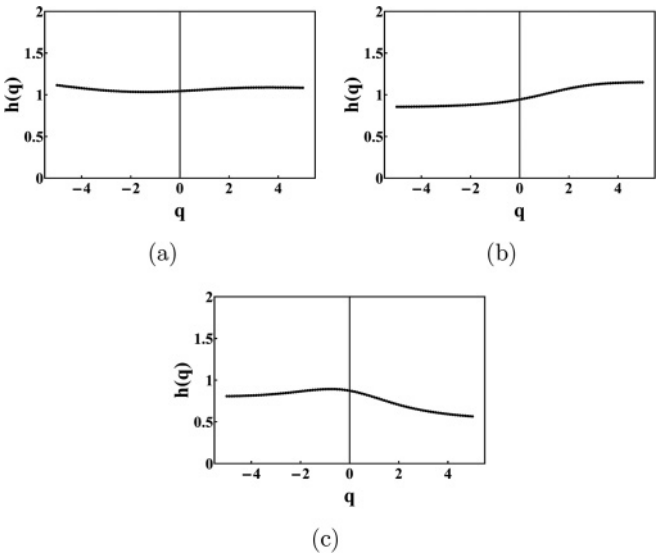

FIG. 18. (a) Cross section of the $h(q,s)$ dependence for healthy subject CHM, taken for scale $s = 30$. (b) The cross section for $s = 75$ and (c) for $s = 360$.

heart disease at risk of cardiac arrest (BHD) who, before the recording analyzed here was made, had suffered two cardiac arrests and now wears an implantable cardioverter device. CHM is the sex, age, and disease matched control pair for BHD used in our earlier study [21].

We also show that $h(q,s)$ for the heart rate variability obtained after a successful, nine months pharmacological treatment after cardiac arrest of the post-myocardial infarct patient DWD [Fig. 20(b)], except for the small scale range, resembles that for the healthy subject CHM [cf. Fig. 8(a)]. The difference visible in Fig. 20(b) between DWD and CHM at small scales is due to a certain number of arrhythmias that still occur [Fig. 20(c)] in spite of the pharmacological treatment and do not occur in the CHM case. Compare with the raw data in Fig. 13(a) recorded in DWD just before his cardiac arrest and subsequent resuscitation. Note that DWD is 64 years old. In spite of this—except for the well-localized effect of arrhythmia on the $h(q,s)$ surface—the results obtained after pharmacological treatment [Fig. 20(b)] compare well with those for the 25-year-old healthy subject in Fig. 8(a). This indicates that the template that we have attempted to define in this paper is a useful concept.

VII. CONCLUSIONS

We present a generalization of the MF-DFA method called multiscale multifractal analysis (MMA). The method allows us to extend the description of the properties of the fluctuations of a signal depending on their magnitude and the time scale (frequency band) at which they occur, using the generalized dependence of the local Hurst exponent on the scale: the surface $h(q,s)$. On this surface, the results of the standard DFA method are represented by one (or two) single points corresponding to the exponent α. The results of standard MF-DFA are represented by a single line: a cross section of $h(q,s)$ at a constant s.

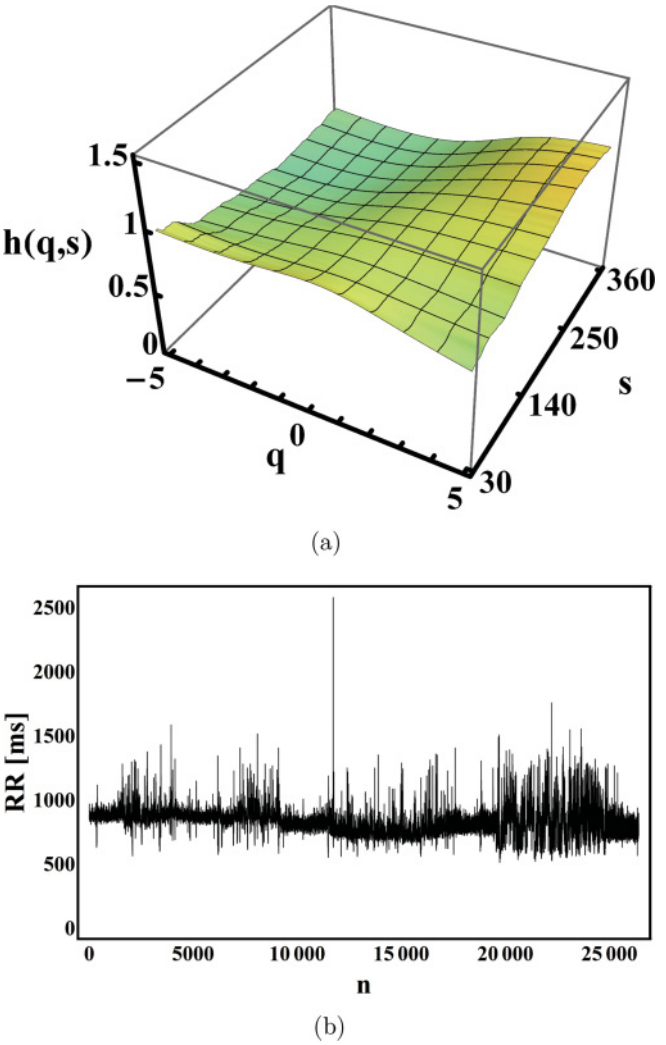

FIG. 19. (Color online) (a) $h(q,s)$ dependence for a 25-year-old man at risk of cardiac arrest (BHD) but without an organic heart disease [cf. Fig. 8(a)]. (b) RR interval series for BHD.

MMA eliminates the need for initial assumptions about the presumed time scale of the investigated problem. The new method is able to characterize monofractality or multifractality of the time series in a wide range of frequencies (scales) simultaneously and may be easily applied to data with strong crossover properties. It may be used with data set lengths down to 15 000 data points in the case of multifractality stemming from correlations. In the case of multifractality due to the properties of the distribution of the series, this number rises to 20 000 data points, because rare events in fat tails of distribution do not have a sufficient representation, and, in fact, the distribution is different from the complete Cauchy distribution. In general, when analyzing data with unknown distribution properties, we have to use a time series of at least 20 000 points. We found that the method is relatively resistant to observational noise and nonstationarities, including those in the form of inclusions into the time series of a different dynamics such as arrhythmic events. For heart rate variability analysis of clinical data, the latter feature of MMA allows us to analyze data with at least up to 15% of arrhythmia events—an improvement compared with the less than 5% usually assumed.

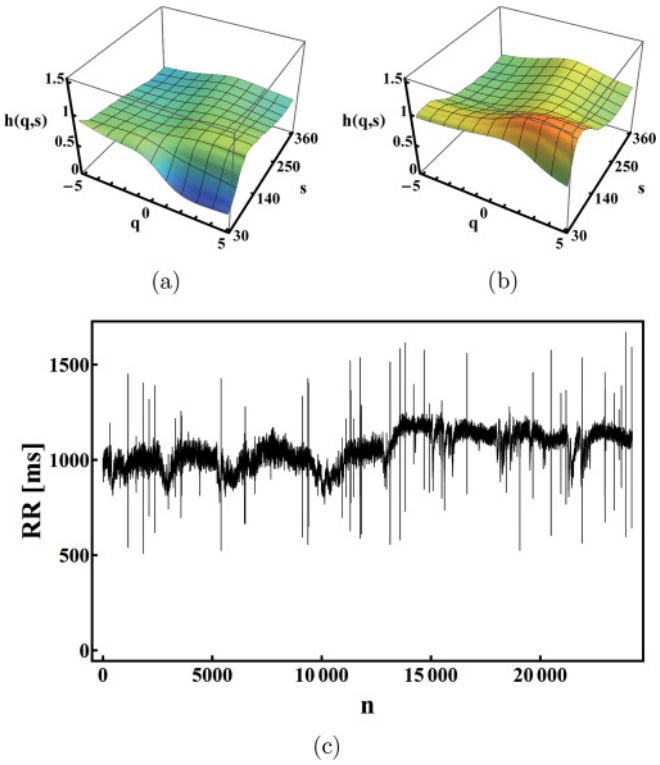

FIG. 20. (Color online) (a) $h(q,s)$ for a subject at risk of cardiac arrest (DWD); cardiac arrest occurred about 1 h after the time series analyzed. (b) $h(q,s)$ for the same subject but after a very successful, nine-month pharmacological treatment. (c) The nighttime RR interval series of the subject DWD after successful pharmacological treatment, the fragment analyzed in (b).

We show that MMA can correctly recognize fractal properties of time series even for relatively small scales, and that it is capable of properly recognizing different fractal properties in small and large scales simultaneously.

To calculate the $h(q,s)$ surface, we use the scale range $s \in \langle 30,360 \rangle$ while, usually, the mean RR interval in a nighttime series is approximately 1 s. Thus, the approximate range of the frequencies we are analyzing is 0.003–0.03 Hz. As defined in the standard guidelines for heart rate variability diagnostics [35], this frequency range corresponds to the very low frequencies band (VLF defined as 0.003–0.04 Hz). This clinically accepted guidelines document—based on linear signal analysis methods—stated in 1996 that, "although the ULF and VLF components account for the remaining 95% of total power, their physiological correlates are still unknown" and that their interpretation needs further development. In the literature, there is a wide discussion about the interpretation of this frequency range. There are some interpretations suggesting that in the VLF band, one can find the effect of thermoregulation [36], the renin-angiotensin-aldosterone system [37], baroreflex, chemoreflex, and abnormalities such as sleep apnea and Cheyne-Stokes respiration [38,39], or that parasympathetic mechanisms play the main role in this frequency range [37,40]. It is likely that all these interpretations are correct, and information about all these phenomena may be found within the VLF range. Up to now, a direct medical interpretation of any kind of results obtained in the VLF range (and also in the ULF band) was difficult as the only method used to assess properties of this band was a power spectrum, and in the power spectrum ULF and VLF merge into a single peak. In spite of this difficulty, VLF power is used in medical diagnostics. MMA is therefore a method that allows us to assess the correlation properties (cf. Sec. VI B) of heart rate variability as a function of the scale (frequency range) and of the magnitude of the fluctuations. We believe that this approach can be very useful in ascertaining the meaning of the VLF component of heart rate variability.

We show that human heart rate variability not only has multifractal properties but also that these properties depend on the time scale, which is related to the frequency band of the signal. This dependence may be far more complex than it is usually assumed and, in general, differs very much from subject to subject. Since the method is relatively insensitive to nonstationarities in the signal, MMA does not require arrhythmia filtering to analyze RR interval series: the effects of arrhythmia are readily recognizable in the properties of the $h(q,s)$ surface. This is, in our opinion, an important issue that is also of promising medical value—a lot of cases are eliminated from HRV analysis because of arrhythmias. Preliminary tests showed that the method may allow us to detect the risk of cardiac arrest also for subjects without any organic heart disease.

ACKNOWLEDGMENTS

The paper was supported by the Polish Ministry of Science, Grant No. 496/N-COST/2009/0 up to September 2011.

[1] K. Kiyono, Z. R. Struzik, N. Aoyagi, F. Togo, and Y. Yamamoto, Phys. Rev. Lett. **95**, 058101 (2005).
[2] C.-K. Peng, J. Mietus, J. M. Hausdorff, S. Havlin, H. E. Stanley, and A. L. Goldberger, Phys. Rev. Lett. **70**, 1343 (1993).
[3] R. Fischer, M. Akay, P. Castiglioni, and M. Di Rienzo, Med. Biol. Eng. Comput. **41**, 543 (2003).
[4] Z. R. Struzik, J. Hayano, S. Sakata, S. Kwak, and Y. Yamamoto, Phys. Rev. E **70**, 050901 (2004).
[5] P. C. Ivanov, L. A. N. Amaral, A. L. Goldberger, S. Havlin, M. G. Rosenblum, Z. R. Struzik, and H. E. Stanley, Nature (London) **399**, 461 (1999).
[6] L. A. Nunes Amaral, P. C. Ivanov, N. Aoyagi, I. Hidaka, S. Tomono, A. L. Goldberger, H. E. Stanley, and Y. Yamamoto, Phys. Rev. Lett. **86**, 6026 (2001).
[7] D. Makowiec, R. Gałąska, A. Dudkowska, A. Rynkiewicz, and M. Zwierz, Physica A **369**, 632 (2006).
[8] C.-K. Peng, S. V. Buldyrev, S. Havlin, M. Simons, H. E. Stanley, and A. L. Goldberger, Phys. Rev. E **49**, 1685 (1994).
[9] H. E. Hurst, Trans. Am. Soc. Civ. Eng. **116**, 770 (1951).
[10] J. Feder, *Fractals* (Plenum Press, New York, 1988).
[11] H. E. Stanley and P. Meakin, Nature (London) **335**, 405 (1988).
[12] B. J. West and N. Scafetta, Phys. Rev. E **67**, 051917 (2003).

[13] L. Telesca, G. Colangelo, V. Lapenna, and M. Macchiato, Chaos Solitons Fractals **18**, 385 (2003).
[14] Z.-Y. Su and T. Wu, Physica D **221**, 188 (2006).
[15] M. Petelczyc, J. J. Żebrowski, R. Baranowski, and L. Chojnowska, Physiol. Meas. **31**, 1635 (2010).
[16] M. Petelczyc, J. J. Żebrowski, and R. Baranowski, Phys. Rev. E **80**, 031127 (2009).
[17] K. Klimaszewska and J. J. Żebrowski, Phys. Rev. E **80**, 026214 (2009).
[18] T. Buchner, M. Petelczyc, J. J. Żebrowski, A. Prejbisz, M. Kabat, A. Januszewicz, A. J. Piotrowska, and W. Szelenberger, Chaos **19**, 028504 (2009).
[19] J. J. Żebrowski, K. Grudzinski, T. Buchner, P. Kuklik, J. Gac, G. Gielerak, P. Sanders, and R. Baranowski, Chaos **17**, 015121 (2007).
[20] J. J. Żebrowski and R. Baranowski, Phys. Rev. E **67**, 056216 (2003).
[21] J. J. Żebrowski, W. Popławska, and R. Baranowski, Phys. Rev. E **50**, 4187 (1994).
[22] *Mayo Clinic Cardiology: Concise Textbook*, edited by J. G. Murphy and M. A. Lloyd (Mayo Clinic Scientific Press, Rochester, 2007).
[23] J. W. Kantelhardt, S. A. Zschiegner, E. Koscielny-Bunde, S. Havlin, A. Bunde, and H. E. Stanley, Physica A **316**, 87 (2002).
[24] M. Schroeder, *Fractals, Chaos, Power Laws: Minutes from an Infinite Paradise* (Freeman, New York, 1992).
[25] J. F. Muzy, E. Bacry, and A. Arneodo, Phys. Rev. Lett. **67**, 3515 (1991).
[26] A. Saichev and D. Sornette, Phys. Rev. E **74**, 011111 (2006).
[27] See Supplemental Material at http://link.aps.org/supplemental/10.1103/PhysRevE.85.021915 for two animations. The first animation shows how the fluctuations of $F_q(s)$ can change $h(q)$ and $f(\alpha)$. On the top panel, the $F_q(s)$ curves family can be seen. Blue solid lines show the current window of fitting, and the fitting is shown as red dashed lines. The fitting window length starts always at a scale $s = 10$ and expands. Because of the substantial fluctuations of the $F_q(s)$ values, even a slightly wider window of fitting can cause drastic changes in the resulting $h(q)$ and $f(\alpha)$. The second animation depicts the emergence of $h(q,s)$. On the top panel, a family of curves $F_q(s)$ with the moving fitting window (blue solid lines) together with the straight line fits (red dashed lines) can be seen. On the bottom panel, the resulting $h(q)$ is shown. Every $h(q)$ shown is a cross section of the $h(q,s)$ dependence at constant s.
[28] J. W. Kantelhardt, E. Koscielny-Bunde, H. H. A. Rego, S. Havlin, and A. Bunde, Physica A **295**, 441 (2001).
[29] W.-X. Zhou and D. Sornette, Physica A **388**, 2623 (2009).
[30] K. Hu, P. C. Ivanov, Z. Chen, P. Carpena, and H. E. Stanley, Phys. Rev. E **64**, 011114 (2001).
[31] J. Ludescher, M. I. Bogachev, J. W. Kantelhardt, A. Y. Schumann, and A. Bunde, Physica A **390**, 2480 (2011).
[32] A. Y. Schumann and J. W. Kantelhardt, Physica A **390**, 2637 (2011).
[33] C.-K. Peng, S. Havlin, H. E. Stanley, and A. L. Goldberger, Chaos **5**, 82 (1995).
[34] P. Castiglioni, G. Parati, C. Lombardi, L. Quintin, and M. D. Rienzo, Biomed. Tech. **56**, 175 (2011).
[35] Task Force of The European Society of Cardiology and The North American Society of Pacing and Electrophysiology, Circulation **93**, 1043 (1996).
[36] R. I. Kitney, J. Physiol. **229**, 40 (1973).
[37] *Practical Signal and Image Processing in Clinical Cardiology*, edited by J. J. Goldberger and J. Ng (Springer, London, 2010).
[38] D. P. Francis, L. C. Davies, K. Willson, P. Ponikowski, A. J. S. Coats, and M. Piepoli, Clin. Sci. **99**, 125 (2000).
[39] P. Ponikowski, T. P. Chua, M. Piepoli, D. Ondusova, K. Webb-Peploe, D. Harrington, S. D. Anker, M. Volterrani, R. Colombo, G. Mazzuero, A. Giordano, and A. J. S. Coats, Circulation **96**, 2586 (1997).
[40] J. A. Taylor, D. L. Carr, C. W. Myers, and D. L. Eckberg, Circulation **98**, 547 (1998).